Acoustic field variability induced by internal solitary waves on a continental shelf

S. Finette, R. Oba

Acoustics Division, Naval Research Lab, Washington, DC 20375 USA.
finette@wave.nrl.navy.mil, roba@wave.nrl.navy.mil

Abstract

We have performed computer simulations of acoustic field variability in a continental shelf, shallow water environment for which volumetric sound speed fluctuations were present in the form of an anisotropic internal wave field. The anisotropic field was described by a solitary wave packet. Horizontal refraction from higher sound speed thermocline depressions to lower sound speed regions between depressions is illustrated. The refraction is responsible for beam wander and beam splitting that occurs while beamforming on a horizontal array in this environment.

1. Introduction

Fluctuations of the volumetric sound speed field in shallow water represent a significant contribution to acoustic field variability. While these fluctuations are typically less than one percent of the mean sound speed in the water column, they can have a significant effect on the amplitude and phase of an acoustic field propagating in this environment over relatively short range [1-4]. Phase-sensitive array processing schemes, such as plane wave or matched field beamforming, are quite sensitive to this variability since perturbations of the mean sound speed distribution lead to degradation of spatial acoustic coherence and therefore introduce error into the processing schemes. We report here on beamforming errors that are directly attributed to horizontal refraction of the acoustic field caused by oceanographic variability in the form of solitary internal gravity waves located within a typical continental shelf ocean environment. It was assumed that the acoustic field propagated on the shelf in a region located some distance from the shelf-break origin of these internal waves, where the latter are commonly generated by tidal flow through stratified water. After generation near the shelf-break, an internal tide often evolves into the form of a solitary wave packet or undular bore that propagates shoreward at a speed of approximately 0.5-1.0 m/s. Interaction of the acoustic field with the internal wave field is of interest here, and results from computer simulation are presented. The internal wave model is briefly described in the next section, followed by a discussion of the acoustic modeling approach. Some representative results are then given to illustrate the interaction between an internal wave field and an acoustic field in the context of plane wave beamforming on a horizontal array.

2. Description of the Model

A data-constrained model of the ocean environment was developed from data acquired on the New Jersey shelf during the SWARM95 experiment [5]. The sound speed field was specified as a function that represented a dominant summer thermocline with additional, small perturbation terms corresponding to space-time variations of the internal wave field. Define the coordinates $\{x,y\}$ to represent position in a plane parallel to the ocean surface and let water depth be denoted by z. A three-component model of the sound speed distribution can then be written in the form [2]

$$c(x,y,z,t) = \bar{c}(x,z) + \delta c_B(x,y,z,t) + \delta c_S(x,z,t) \qquad (1)$$

where $\bar{c}$ is a mean, time-independent profile representing a summer thermocline with mild range dependence and the two perturbation terms correspond to a spatially diffuse background internal wave field δc_B and the solitary wave packet contribution δc_S. The background term was horizontally isotropic, and consisted of a sum over plane harmonic waves propagating in different azimuthal directions with a depth dependence given by the lowest order (mode one) eigenfunction of the internal wave field. This depth dependence is typical of continental shelf environments. The energy distribution among the plane waves was determined by Monte Carlo sampling of the measured internal wave displacement power spectrum for this shallow water region. On the other hand, the solitary wave contribution was horizontally anisotropic, with wave crests oriented parallel to the y-axis; the packet did not depend on the cross-range coordinate, y, since it was chosen to propagate in the x-direction. It was

TG Leighton, GJ Heald, HD Griffiths, G Griffiths, (eds.), 'Acoustical Oceanography', Proc. Institute of Acoustics Vol. 23 Part 2, 2001.

assumed that the wave packet's space and time evolution could be represented approximately by a solution of the standard Kortewig de Vries (KdV) equation [2]. Note that while this contribution has a non-linear origin in the hydrodynamics, it was assumed that the non-linearity was weak enough so that the resulting sound speed perturbation approximately satisfied the linearity assumption implicit in Equation (1). The non-linearity and dispersion parameters associated with the KdV equation, as well as the depth-dependent modal structure of the internal wave field, were estimated from the experimental data. The total sound speed distribution evolved in integer time increments $t = n\Delta t$, where Δt represented an interval of one minute. The resulting set of environmental snapshots was computed for a 15 km x 15 km region, with a constant water depth of 68 m overlying 10 m of sediment and an absorbing bottom. Each snapshot was input to a 3-D wide-angle parabolic equation code that was used to propagate the acoustic field from a point source through an azimuthal wedge bounded by the ocean surface and bottom [6]. This code was implemented with a finite difference scheme, and used discrete differential operators to represent wide-angle propagation in elevation and narrow-angle azimuthal coupling. The rationale for performing 3-D acoustic calculations was based on the assumption that anisotropic correlation lengths associated with the wave packet contribution could induce significant horizontal refraction of energy. This effect cannot be represented by a set of N range-depth (a.k.a. Nx2D) calculations of the acoustic field for different azimuthal directions since such computations do not include azimuthal coupling of energy. The next section presents some results of the 3-D acoustic calculations.

3. Results

We first consider an example of the time evolution of the acoustic transmission loss and horizontal spatial coherence as a function of range and cross-range for three representative environmental snapshots. The cross-range (horizontal) spatial coherence is defined here by the expression [6]

$$C_\phi(r,z,\chi) = \frac{\left|\left\langle p(r,z,0)p^*(r,z,\chi)\right\rangle\right|}{\sqrt{\left\langle\left|p(r,z,0)\right|^2\right\rangle\left\langle\left|p(r,z,\chi)\right|^2\right\rangle}} \quad . \tag{2}$$

The acoustic field p is written in terms of a range variable $r = \sqrt{x^2 + y^2}$, where $r = 0$ corresponds to the location of an acoustic point source. The variable r also represents the magnitude of the vector **b** described below. The cross-range χ lies normal to r and was measured relative to the point $\chi = 0$, which corresponded to a point lying along r. Therefore, a cross-range was defined for each value of r. The symbol * denotes complex conjugation. The brackets indicate temporal averaging over environmental snapshots for some specified time window. For a depth z, Equation (2) expresses the normalized horizontal coherence at range r between two points separated in cross-range by a distance χ, and parametrized by the angle ϕ. This parameter represents the angle between the wave packet propagation vector and the central angle of propagation of the acoustic field within the azimuthal wedge, as illustrated in the lower left hand corner of Figure 1.

Referring to this figure, the three volumes on the left show environmental snapshots corresponding to the times given on the right side of the figure. The volumes illustrate both the thermocline associated with the mean sound speed and the sum of the background and solitary wave field components, as well as a cutaway interior view of a section of the sound speed distribution. The white dots in the snapshots represent an acoustic point source of 400 Hz located at a depth of 30 m. Within the volumes, the intersecting planes illustrate the boundaries of an acoustic propagation wedge subtending an opening of 30 degrees. The wedge insert at the bottom left hand side defines the angle ϕ between the vectors **a** and **b**. Vector **a** is pointing in the direction of propagation of the solitary wave packet and **b** bisects the wedge aperture with $|\mathbf{b}| = r$. For the environmental snapshots shown in Figure 1, the angle ϕ is 90 degrees, indicating acoustic propagation primarily parallel to the wave crests of the solitary wave packet. The thermocline depressions associated with the packet were approximately 10 m peak-to-trough with a pulse width of about 200 m and a separation distance of 450-500 m between the first few adjacent depressions. Note that in the lower left snapshot, the wave packet was exterior to the propagation wedge, and for subsequent snapshots the packet partially overlapped the wedge. The three figures to the right of each snapshot represent planar projections of the depth-averaged sound speed, transmission loss (TL) and spatial coherence as a function of range and cross-range from the acoustic source. Each projection was acquired from a rectangular area that was centered within the propagation wedge and the projected views in the figure are looking downward toward the ocean surface. The sound speed and transmission loss were computed at the time specified to the right, while the coherence was computed by averaging the field over snapshots taken from a 36 minute sliding window where the first 35 minutes preceded the indicated time. The last environmental snapshot used to form the average corresponded to the depth-averaged sound speed and transmission loss shown.

At time $t = 0$ the solitary wave packet was exterior to the propagation wedge as noted above. The only contributions to the sound speed field that affected acoustic propagation were those corresponding to the thermocline and the perturbation due to the isotropic background internal wavefield. The corresponding depth-averaged transmission loss was approximately uniform in cross-range with weak variability of 1-2 dB. The horizontal coherence in that environment was high over the range 2.5-10 km. This indicated that the environment introduced no significant degradation in phase over a time during which only the background internal wave field perturbed the thermocline. The situation changed a few minutes later as the first thermocline depression of the solitary wave packet entered the propagation region; an example is shown in the middle set of three projections corresponding to time t = 14 min. The sound speed variations associated with the leading depression are now visible in the depth-averaged sound speed projection, and the horizontal refraction of energy from this sound speed perturbation is illustrated in the corresponding transmission loss projection. Both significant focusing and defocusing of the acoustic intensity are evident, as energy was transferred from high sound speed regions to low sound speed regions. Focusing decreased the depth-averaged transmission loss by 5-10 dB relative to background levels (taken as those levels at t = 0), while transmission loss in the shadow (defocused) region was some 5 dB higher than background levels. During that time the horizontal spatial coherence began to decrease, indicating that some phase degradation had occurred between cross-ranges $\chi = 0$ and $\chi = 0.5$ km. This corresponded to the region initially affected by horizontal refraction of energy from the first thermocline depression. Degradation of the cross-range coherence continued as the packet traversed the propagation wedge so that, by t = 27 min, the spatial coherence had dropped significantly. This time corresponded to an environment in which the first two thermocline depressions were present within the propagation wedge, with horizontal refraction from both depressions combining to give a strong range dependent focusing of energy between the thermocline depressions.

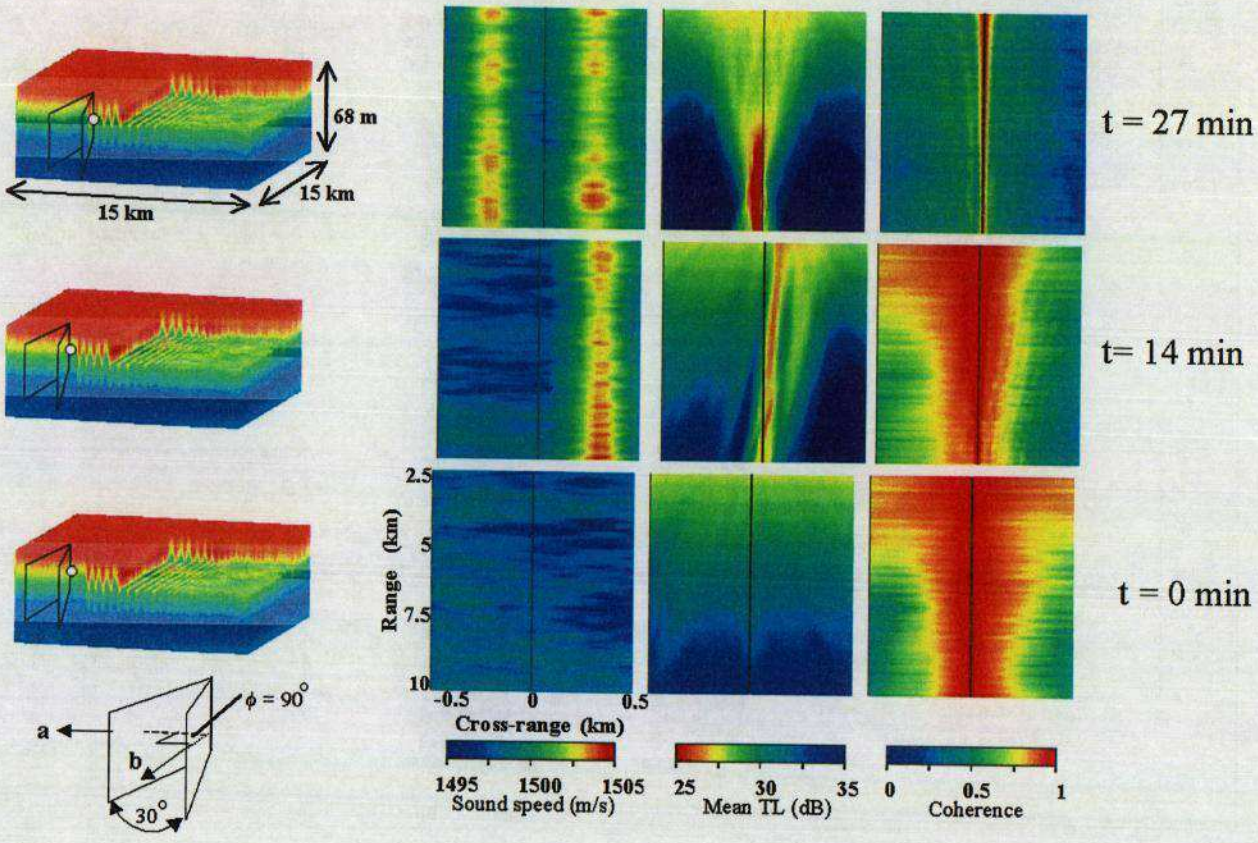

Figure 1. Environmental snapshots taken 14 minutes apart, along with the corresponding depth-averaged projections of sound speed, transmission loss (TL) and spatial horizontal coherence. The projections are viewed from the ocean surface looking down into the wedge. Propagation was primarily parallel to the wave crests, within the propagation wedge illustrated in the snapshots. The acoustic source is located on the black lines at zero range. The sound speed color bar also represents the sound speed distribution in the snapshot volumes.

The solitary wave packet effectively acted like a natural oceanographic waveguide that preferentially funneled energy between thermocline depressions. For angles $\phi < 70$ degrees, horizontal refraction was insignificant and both the intensity focusing and coherence degradation were negligible [6]. Results obtained for a shallow source (z = 5 m) were qualitatively similar. We conclude that a non-stationary, anisotropic focusing of acoustic energy can occur for propagation roughly parallel to the wave crests and can lead to significant loss of spatial coherence. These effects are a direct result of the anisotropic correlation lengths associated with the solitary wave packet, even though the sound speed perturbation of the thermocline is small ($\frac{\delta c_s}{\bar{c}} \leq 10^{-2}$).

Within this anisotropic environment, beamforming using a horizontal array exhibited sensitivity to array orientation relative to the direction of packet propagation. This orientation was described by the azimuthal angle formed between the cross-range direction in which coherence was computed (at fixed array depth of 35 m) and the direction of propagation of the wave packet. An example of plane wave beamforming is illustrated in Figure 2 for a case where acoustic field directionality is measured for a source located at broadside with respect to a fixed horizontal array. For this geometry, the packet's propagation vector was selected such that the solitary wave

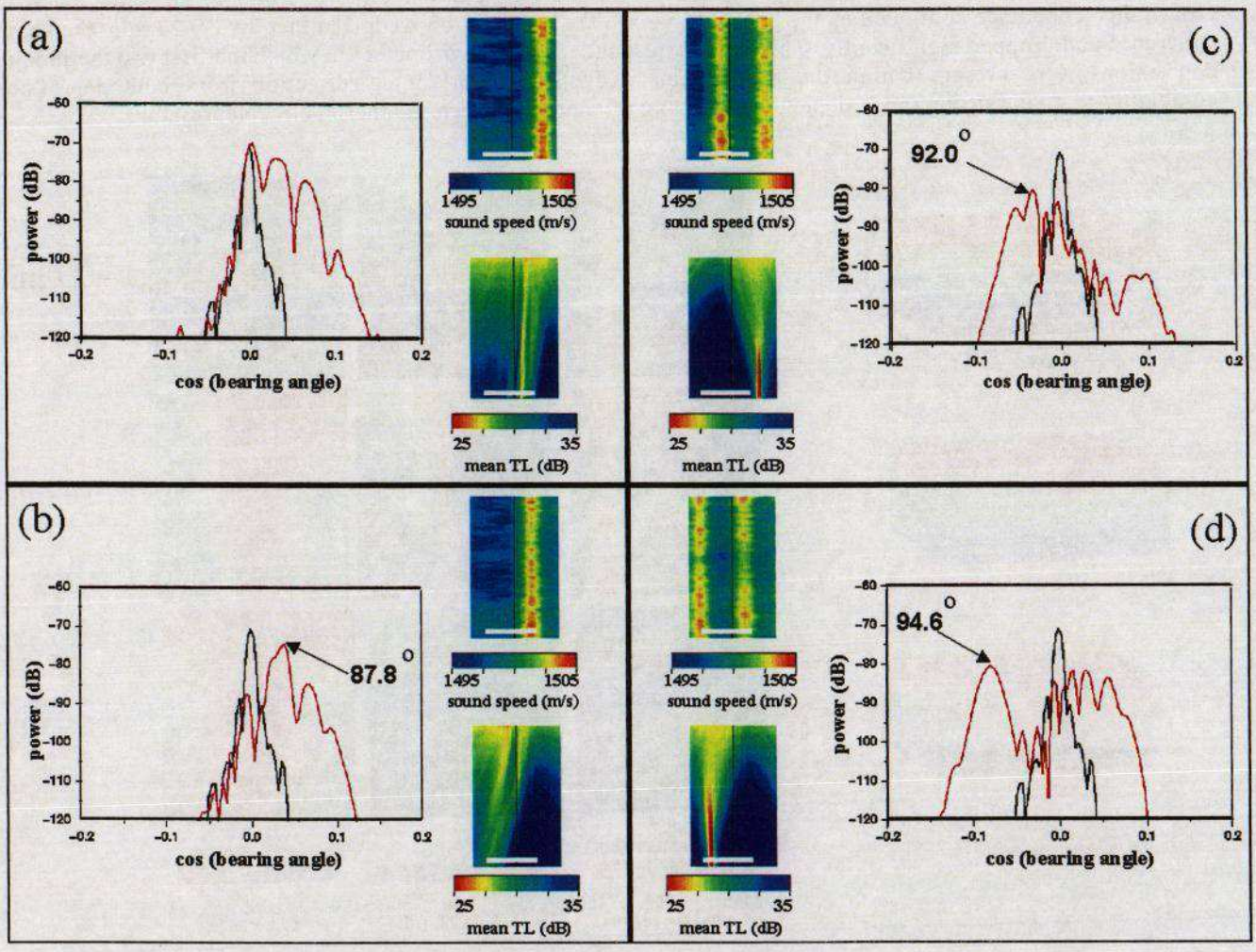

Figure 2. Beam power as a function of time, for different positions of the internal wave packet within the propagation wedge. The true source location was at broadside, and the horizontal array was located at a fixed range of 10 km from the source, at a depth of 30 m. Both beam splitting and beam wander were correlated with the position of the packet depressions relative to the array. The inserts show the depth-averaged projections of sound speed and transmission loss at the time the beam power was calculated. The bearing angle convention is that angles ≤ 90 imply wave fronts approaching from the right hand side of the TL plots. Broadside is 90 degrees. The inserts have the same spatial scales as shown in Figure 1, though the aspect ratio has been modified. Times associated with the snapshots correspond to (a) 14 minutes (b) 18 minutes (c) 24 minutes and (d) 31 minutes.

crests are aligned normal to the array orientation. This configuration is shown in the color inserts, which have the same interpretation and scale as in Figure 1. A white horizontal line depicts the orientation, length and position of the horizontal array on which the beamformed power was computed. The array was comprised of 481 sensors spaced 1.25 m apart and yielded an aperture of 160λ for an acoustic frequency of 400 Hz. The four parts of this figure depict the beam power on the array as a function of time during which a solitary wave packet passed through the region. The array was located 10 km from the source and within the near-field. Therefore, a wavefront curvature correction was applied to the beamformer computations. Beamforming was performed on a single time-evolving realization of the ocean environment. Owing to the non-stationary nature of this environment, no averaging was performed to compute the beam power. In each beam plot, the black curve represents beam power for the case in which only the isotropic background internal wave field was present. Under such conditions, the beamformer correctly estimated the bearing of the source (located at broadside) and the beamwidth was consistent with that for a diffraction limited aperture. The red curves correspond to the beam power for the instantaneous sound speed environment shown in the inserts in Figure 2(*a-d*); these cases contained the solitary wave packet within the propagation wedge. Referring to Figure 2(*a*), the first thermocline depression had just reached the right hand edge of the array. While the source was correctly estimated to be located at broadside, there was significant beam spread introduced by refraction of energy off the thermocline depression. In addition, multiple peaks are clearly visible and are most likely due to modal arrivals from different azimuthal directions, though a modal decomposition of the field would be necessary to confirm this tentative conclusion. Beam wander is illustrated in Figures 2(*b,c*) as the packet progressed across the array, with a 10 dB drop in peak beampower shown in Figure 2(*c*). This drop in level was associated with the shadow zone arising from scattering of the acoustic field off the depression when the acoustic source is near to or within the depression. Beam splitting is illustrated in Figure 2(*d*), during which time two depressions were significantly refracting the acoustic field at the array. The packet effectively altered the true direction of arrival by as much as 4.5 degrees due to horizontal refraction. In contrast, a bearing variation of the peak beam power of only a few tenths of a degree occurred when only the isotropic internal wave component was present and propagating through the wedge.

4. Conclusions

This paper described some results of 3-D computer simulations involving the propagation of acoustic waves through a continental shelf environment that included volume variability in the form of internal gravity waves. The presence of an anisotropic internal wave field induced a corresponding azimuthal dependence on the acoustic field propagating through the waveguide. This dependence caused a focusing of energy between thermocline depressions comprising a solitary wave packet, as well as a loss of cross-range spatial coherence of the acoustic field. The coherence loss and energy focusing were non-stationary effects due to horizontal refraction of energy from the (high sound speed) thermocline depressions to the lower sound speed region between depressions. The drop in acoustic field coherence appeared as beam wander and beam splitting when interpreted in the context of beamforming on a fixed horizontal array with broadside oriented normal to the wave packet's propagation vector. We note that for other orientations of the array relative to the direction of propagation of the packet, the beamforming errors discussed in the previous section dropped off rapidly. Some recent theoretical work [7] on propagation through planar and curved solitary wave packets supports the results presented here and shows that the effects are stable for mild curvature of the solitary wave front.

5. Acknowledgment

This research was supported by the Office of Naval Research.

6. References

[1] Tielbuerger D, Finette S and Wolf S N. Acoustic propagation through an internal wave field in a shallow water waveguide. *J. Acoust. Soc. Am.* 1998; **101**: 789-808

[2] Finette S, Orr M H, Turgut A, Apel J, Badiey M, Chiu C S, Headrick R H, Kemp J N, Lynch J F, Newhall A E, von der Heydt K, Pasewark B, Wolf S N and Tielbuerger D. Acoustic field variability induced by time-evolving internal wave fields. *J. Acoust. Soc. Am.* 2000; **108**: 957-972

[3] Lynch J, Jin G, Pawlowicz R F, Ray D, Plueddemann A J, Chiu C S, Miller J H, Bourke R H, Rost Parsons A and Muench R. Acoustic travel-time perturbations due to shallow water internal waves and internal tides in the Barents sea polar front: Theory and experiment. *J. Acoust. Soc. Am 1996;* **99**: 803-821

[4] Rubenstein D. Observations of Cnoidal Internal Waves and their Effect on Acoustic Propagation in Shallow

Water. *IEEE J. Oceanic Eng* 1999; **24**: 346-357

[5] Apel J R, Badiey M, Chiu C S, Finette S, Headrick R, Kemp J, Lynch J F, Newhall A, Orr M H, Pasewark BH, Tielbuerger D, Turgut A, von der Heydt K and Wolf S. An overview of the 1995 SWARM shallow-water internal wave acoustic scattering experiment. *IEEE J. Oceanic Eng.* 1997; **22**: 465-500

[6] Oba R and Finette S. Acoustic Propagation Through Anisotropic Internal Wave Fields: Transmission Loss, Cross-Range Coherence and Horizontal Refraction. Submitted to *J. Acoust. Soc. Am.*

[7] Katsnel'son B G and Pereselkov S A. Low-frequency horizontal acoustic refraction caused by internal wave solitons in a shallow sea. *Acoustical Physics* 2000; **46**: 779-788